

1

2 **1. Abstract**

3

4 The accessible porosity for Cl^- in bentonite is smaller than the the total porosity due to anion
5 repulsion (exclusion) by the surface of montmorillonite, the main mineral in bentonite. The
6 accessible porosity is a function of the bentonite density and the salt concentration. Anion
7 exclusion data were gathered from the literature, reprocessed in a coherent data set, and
8 modelled using four different models. Very simple models, with or without anion access to
9 the interlayer space, are successful in reproducing trends in anion exclusion in bentonite as a
10 function of ionic strength in the external solution and montmorillonite bulk dry densities in
11 the bentonite. However, a model that considers clay microstructure changes as a function of
12 bentonite compaction and ionic strength is necessary to reproduce observed trends in the data
13 for all experimental conditions within a single model. Our predictive model excludes anions
14 from the interlayer space and relates the interlayer porosity to the ionic strength and the
15 montmorillonite bulk dry density. This presentation offers a good fit for measured anion
16 accessible porosities in bentonites over a wide range of conditions and is also in agreement
17 with microscopic observations.

1

2

3 **2. Introduction**

4 Bentonite is foreseen as a barrier material in radioactive waste repositories and the properties
5 of this material are currently under investigation (NAGRA., 2002; ANDRA, 2005; Nykyri et
6 al., 2008). Bentonite has a high proportion of Na-montmorillonite, a clay mineral that swells
7 in water and endows bentonite with a very low hydraulic conductivity. As a result, transport
8 of water and solutes in bentonite is mainly diffusive, with diffusion coefficients that are much
9 smaller than in bulk water, in particular for anions (Kozaki et al., 1998a; Kozaki et al., 1998b;
10 Madsen, 1998; Kozaki et al., 2001; Ochs et al., 2001; Bourg et al., 2007; Van Loon et al.,
11 2007; Kozaki et al., 2008). Natural clay formations that are currently under investigation for
12 waste repository exhibit similar diffusion properties due to their low porosity and significant
13 content in swelling clay minerals (Descostes et al., 2008). Anions carry the potentially highest
14 risk in the radioactive waste (Altmann, 2008; Grambow, 2008), and their behaviour and
15 transport in the porespace of engineered or natural clay materials must be quantified in
16 models that can be used in transport codes. The present study focuses on bentonite properties
17 with the hope to further extent this work to natural clay-rock formations.

18 In clay materials, the dominant transport mode is diffusive and a function of the concentration
19 gradient, activity corrections (activity coefficient of solution species and complexation in
20 solution), the mobility of the species in water (D_w), charging due to different mobilities or
21 electrical current, the accessible porosity (ε), the tortuosity (the length of the actual path over
22 the straight line distance) and the retardation as a result of reactions such as sorption or ion
23 exchange. Diffusion experiments data can be fitted with transport models that account for
24 these variables, and the results provide effective diffusion coefficients (D_e) for Fick's law. For

1 an homogeneous medium and for anions without retardation such as Cl⁻, Fick's law simplifies
2 to:

$$\frac{\partial c}{\partial t} = D_e \frac{\partial^2 c}{\partial x^2} \quad \text{Equation 1}$$

3 The effective diffusion coefficient is related to the anion tracer diffusion coefficient in anion
4 accessible porosity (ε_{an}) by

$$D_e = \varepsilon_{an} D_p = \varepsilon_{an} \frac{D_w}{\theta^2} \quad \text{Equation 2}$$

5
6 where D_p is the porewater diffusion coefficient (m²/s), D_w is the anion diffusion coefficient in
7 water (m²/s), and θ^2 is the tortuosity factor (-). The present study focus on models capable of
8 predicting the value of ε_{an} .

9 Montmorillonite, the main constituent of bentonite, is built from layers of oxygen
10 atoms and cations in tetrahedral-octahedral-tetrahedral (TOT) coordination. The structure has
11 an excess of negative charge that is compensated by cations in the interlayer space and on the
12 outer surface. Anions are repelled from the negative surface of montmorillonite and thus,
13 occupy only part of the porespace of bentonite. This part can become very small, almost zero,
14 when the bentonite is highly compacted and the external solution has low ionic strength
15 (Molera et al., 2003; Muurinen et al., 2007; Van Loon et al., 2007). The resulting anion
16 exclusion is well known in soil science (Bouyoucos, 1921; Schofield, 1947). Following
17 Schofield (1947), the Gouy-Chapman (GC) theory for the diffuse double layer at a charged
18 surface, wherein ions are treated as point-like charges, has been applied to model anion
19 exclusion in clay suspensions (Bolt and Warkentin, 1958; Edwards and Quirk, 1962; Edwards
20 et al., 1965; Bolt and De Haan, 1982). Further improvement was achieved by Sposito (1992),
21 who coupled microstructure information to the modified Gouy-Chapman (MGC) equations in
22 which the distances of minimal approach, due to the ion sizes, are taken into account. By

1 considering the stacking size of Na-montmorillonite in suspension (between 1.2 and 1.6 TOT
2 layers are stacked), Sposito could reproduce chloride exclusion data without any adjustable
3 parameters. Muurinen et al. (2007) and Birgersson and Karnland (2009) used the Donnan
4 equation (Donnan and Guggenheim, 1932) to calculate the Cl-concentration in compacted
5 bentonite in contact with an external NaCl solution. In the Donnan calculation, the porespace
6 contains an excess of counter-ions and a deficit of co-ions that balance the surface charge, and
7 at the same time, are in equilibrium with a charge-free external solution. Birgersson and
8 Karnland (2009) modeled their experiments with a single, uniform porosity in the bentonite,
9 but Muurinen et al. (2007) could only fit their data with two porosities in which the surface
10 charge was distributed differently as a function of the bentonite density.

11 It is indeed not very likely that all the porespace in bentonite has uniform
12 electrochemical properties. Figure 1 gives a pictorial presentation how the porespace can be
13 envisioned to contain three different types (Bourg et al., 2003; Bradbury and Baeyens, 2003;
14 Kozaki et al., 2008):

15 Interlayer water (V_{int}) with water and cations between the montmorillonite TOT layers, devoid
16 of anions. The cations compensate the structural charge deficit of the TOT layers, the
17 water molecules are built up in layers and are part of the crystallographic structure of
18 the montmorillonite.

19 Electrostatic double layer (EDL) water (V_{EDL}), containing water, cations and anions; an excess
20 of cations and a deficit of anions neutralize the remaining charge at the outer surface of
21 the montmorillonite. The EDL forms the transition zone from the mineral surface to free
22 porewater.

23 Free porewater (V_{free}), a charge-balanced aqueous solution of cations and anions.

24

1 The proportions of the different water types depend on size and shape of the montmorillonite
 2 flakes in the bentonite and the degree of compaction as expressed by the dry density (*i.e.* the
 3 mass of clay without hydration water divided by the volume containing that clay).
 4 Furthermore, the free porewater composition determines, by electrostatics, the extension of
 5 the diffuse layer in the pore and influences, by osmotic pressure, the interlayer water when the
 6 bentonite density is less than about 1.3 kg/dm³ (Kozaki et al., 2008). The proportions
 7 determine the anion exclusion, which can be expressed as the concentration ratio of an anion
 8 in the overall porespace in bentonite and the external solution. Hence, the experiments of
 9 Muurinen et al., 1989; Molera et al., 2003; Muurinen et al., 2004; Van Loon et al., 2007, who
 10 determined that ratio for NaCl-solutions, can be used to extract the porosity distribution as a
 11 function of packing density and NaCl concentration.

12 Figure 1 also serves to illustrate the steps to be taken for delineating those proportions.
 13 First, the impurities must be subtracted from the solid part since their surface charge is
 14 negligible compared to montmorillonite. Second, the amount of interlayer water must be
 15 defined using the interlayer thickness given by XRD-measurements and the internal surface
 16 area of the montmorillonite. The latter is a function of the stacking number of the TOT layers.
 17 Third, the remaining porosity must be subdivided into a charged fraction and free porewater.
 18 The charged fraction is a function of the surface charge of the montmorillonite and its external
 19 surface area, which can be reduced by the impurities that cover it. Altogether, the constituents
 20 of bentonite sum up to its volume:

$$V_{tot} = \frac{m_{bent} \times (1 - x_{imp})}{\rho_{mm}} + \frac{x_{imp} \times m_{bent}}{\rho_{imp}} + \frac{m_{IL_w}}{\rho_{IL_w}} + \frac{m_{EDL_w}}{\rho_{EDL_w}} + \frac{m_{free_w}}{\rho_{free_w}} \quad \text{Equation 3}$$

21 where V_{tot} is the volume (L), m is the mass (kg), x_{imp} is the mass-fraction of the impurities
 22 (accessory solids) (-), ρ is the density (kg/dm³), and subscript *bent* stands for bentonite, *mm*

1 for montmorillonite, IL_w for interlayer water, EDL_w for EDL water, and $free_w$ for free
 2 porewater (see also Figure 1).

3 This paper will discuss the structure of montmorillonite first, since it determines the
 4 volume of the interlayer porosity and, by the density of interlayer water, its contribution to the
 5 water-filled porosity. Next, the models are presented for calculating anion exclusion, with
 6 model-parameters derived from experiments that allow the Cl-concentration in bentonite
 7 porewater to be calculated as a function of compaction and NaCl concentration in the external
 8 water, and that enable to specify the underlying porosity distribution in the bentonite.

9 **3. Structure and properties of montmorillonite and surface water**

10 **3.1. TOT layer**

11 The effect of size and shape of montmorillonite on the porosity can be calculated by stacking
 12 a montmorillonite unit-cell in 3 dimensions and calculating the internal and external surface.
 13 The chemical formula of a montmorillonite with both tetrahedral and octahedral substitution
 14 is (approximately) $Na_{0.6}[Si_{7.8}Al_{0.2}]^{IV}[Al_{3.6}Mg_{0.4}]^{VI}O_{20}(OH)_4$ (omitting water), with molecular
 15 weight $MW = 733$ g/mol. The presence of iron in the montmorillonite structure increases this
 16 molecular weight. For MX80 montmorillonite fraction, Madsen (1998) reported a MW equal
 17 to 745.2 g/mol. The mineral has a monoclinic unit-cell with dimensions $a \times b \times c^* = 0.516 \times$
 18 0.898×0.94 nm³, where $c^* = c \sin(95^\circ)$ is the orthogonally projected c -axis, d_{001} in XRD
 19 (Madsen, 1998; Bourg, 2004). The crystal density $\rho_{mm} = 2.84$ kg/dm³ for the given unit cell
 20 and MX80 structural formula from Madsen is in agreement with the value reported by Bourg et
 21 al. (2006). A clay crystal is made of unit-cells stacked in three dimensions whose lateral
 22 dimensions are given by $a \times n_a$, $b \times n_b$ and $c \times n_c$.
 23 The external surface area is:

$$A_{ext} = 2 \frac{(n_a \times n_c)(a \times c^*) + (n_b \times n_c)(b \times c^*) + (n_a \times n_b)(a \times b)}{n_a \times n_b \times n_c} \frac{N_A}{MW} \text{ (m}^2\text{/g)} \quad \text{Equation 4}$$

1

2 where $N_A = 6.022 \times 10^{23}$ molecules/mol (Avogadro's number).

3 The internal planar surface is:

$$A_{pl,int} = 2 \frac{a \times b \times (n_c - 1)}{n_c} \frac{N_A}{MW} \text{ (m}^2\text{/g)} \quad \text{Equation 5}$$

4

5 The diameter of montmorillonite flakes in bentonite is about 50-200 nm (Pusch, 2001;
6 Tournassat et al., 2003; Yokoyama et al., 2005; Perronnet et al., 2007; Le Forestier et al.,
7 2010) which means that n_a and n_b are close to 200. The value of n_c ranges from 3 to 7 for Na-
8 montmorillonite in compact materials (Pusch, 2001; Melkior et al., 2009) and 1 to 2 in
9 dispersed suspensions (Sposito, 1992). For $n_a = n_b = 200$ and $n_c = 5$, $A_{ext} = 163 \text{ m}^2\text{/g}$ and $A_{pl,int}$
10 $= 608 \text{ m}^2\text{/g}$. With such small n_c , and high n_a and n_b , the contribution of the edge surface area
11 to the total external surface is relatively small and A_{ext} (Equation 4) can be approximated by:

$$A_{ext} = 2 \frac{a \times b}{n_c} \frac{N_A}{MW} \text{ (m}^2\text{/g)} \quad \text{Equation 6}$$

12 Accordingly, the total specific surface area of montmorillonite (ssa) is approximated by:

$$ssa = 2a \times b \frac{N_A}{MW} \text{ (m}^2\text{/g)} \quad \text{Equation 7}$$

13

14 **3.2. Interlayer water**

15 When montmorillonite expands in water, c^* increases with h_{int} , the interlayer thickness, which
16 is variable and depends on the type of montmorillonite (Slade et al., 1991), the activity of
17 water and the type of cation (Cases et al., 1992; Bérend et al., 1995; Cases et al., 1995; Cases
18 et al., 1997; Ferrage et al., 2005; Ferrage et al., 2007; Ferrage et al., 2010) and on bentonite

1 dry density (Kozaki et al., 1998a; Bourg et al., 2006; Muurinen et al., 2007; Kozaki et al.,
 2 2008). For Na^+ , three distinct spacing's can be observed in XRD-patterns for 1-, 2- and 3-
 3 layer hydrates, with gradual transitions in-between (Slade et al., 1991; Ferrage et al., 2005).
 4 For montmorillonite packed at dry densities varying from 1 to 1.8 kg/dm^3 and in contact with
 5 distilled water, Kozaki et al. (1998a) and Liu et al. (2003) noted d_{001} spacings of 1.88 and 1.56
 6 nm, corresponding to 3- and 2-layer hydrates, respectively, with the transition occurring
 7 between 1.3 and 1.6 kg/dm^3 . With increasing ionic strength (I) up to 0.5 and at a dry density
 8 of 1 kg/dm^3 , Kozaki et al. (2008) observed (i) the appearance of the diffraction peak
 9 corresponding to 2-layer hydrates at $I = 0.1$ and (ii) a slight increase of d_{001} spacing's with
 10 ionic strength as compared to the value determined at "zero" ionic strength. Kozaki et al.
 11 (1998a) could not detect further reduction to a 1-layer hydrate up to 1.8 kg/dm^3 , but González
 12 Sánchez et al. (2008) observed d_{001} spacing lower than the 2-layer hydrate in bentonite
 13 containing more than 95% montmorillonite and packed at 1.9 kg/dm^3 . Only the 3- and 2-layer
 14 hydrates are considered here, since the dry density of 1.9 kg/dm^3 was not attained for
 15 montmorillonite in the experiments treated here.

16 Following Bourg et al. (2006), the interlayer thickness can be calculated from the
 17 Kozaki et al. (1998a; 2008) data as:

$$h_{int} = x_2 h_{int}^{2WL} + x_3 h_{int}^{3WL} \quad \text{Equation 8}$$

18
 19 where h_{int} is the interlayer thickness (m), and x_2 and h^{2WL} (0.62 nm) are the fraction and the
 20 thickness of the 2-layer hydrate, respectively, and similarly for the 3-layer hydrate ($h^{3WL} =$
 21 0.94 nm). The dependence of x_2 on the NaCl concentration is estimated from data reported by
 22 Kozaki et al. (Kozaki et al., 1998a; Kozaki et al., 2001; 2008) and Goto et al. (Goto et al.,
 23 2008): the minimum montmorillonite dry density for the transition from 3WL to 2WL, $\rho_{bd,mm}$
 24 $_{3WL \Leftrightarrow 2WL}$, depends on ionic strength according to $\rho_{bd,mm} \text{ }_{3WL \Leftrightarrow 2WL} = 1.3 - 3 c_{free}$. The

1 montmorillonite dry density corresponding to the end of this transition is 1.6 kg/dm^3 ; between
2 these density values the proportion x_2 is given by:

$$x_2 = \frac{\rho_{bd,mm} - \rho_{bd,mm \text{ 3WL} \leftrightarrow \text{2WL}}}{1.6 - \rho_{bd,mm \text{ 3WL} \leftrightarrow \text{2WL}}} \quad \text{Equation 9}$$

3 Kozaki et al. (2008) observed the concentration effect for a montmorillonite having a density
4 of 1 kg/dm^3 , but noted that montmorillonite acquired a turbostratic structure when packed at
5 lower densities, *i.e.* the basal planes have slipped sideways relative to each other, causing the
6 spacing between planes to be greater than that calculated for an ideal system. As a
7 consequence x_2 and x_3 value cannot be constrained by XRD for low densities.

8 The density of interlayer water can be obtained by combining sample weight and XRD
9 measurements, or it can be calculated, in principle, by molecular dynamics (MD) simulations.

10 The measurements are done by varying the relative humidity (RH) and show a density of 0.7 -
11 0.8 kg/dm^3 for water in the 2-layer hydrate at about 0.8 RH (Cases et al., 1992; Bérend et al.,
12 1995; Ferrage et al., 2007). The results from MD calculations are variable. Karaborni et al.
13 (1996) calculated relative densities of 0.81 and 0.66 for the 2- and 3-layer hydrate,
14 respectively. Others (e.g. Marry et al., 2002) also obtained a decreasing density when
15 interlayer spacing increased. However, interlayer water can be expected to evolve towards the
16 density of free water as spacing increases, and the early numbers may be an artifact due to
17 method approximations (Young and Smith, 2000). More recent calculations have produced
18 densities of about 1 kg/dm^3 for 2WL and 3 WL interlayers, according to water content vs. d_{001}
19 spacing curves (Chavez-Paez et al., 2001; Tambach et al., 2004), the same as for EDL water
20 (Tournassat et al., 2009). Thus, on somewhat uncertain grounds, we assume that the density
21 of the interlayer water is the same as that of EDL and free porewater, *i.e.* 1 kg/dm^3 .

22

23 Figure 2 shows the interlayer porosity ($\varepsilon_{int} = 0.5 S_{int} \times h_{int}$) as a function of the dry density of
24 montmorillonite for $n_c = 3$ and 25, and $c_{\text{NaCl}} = 0.1$ and 1 mol/L in free porewater. First, Figure

1 2 illustrates that the interlayer porosity is a very significant part of the total porosity when dry
2 density increases above 1 kg/dm^3 . This is reached in all practical applications of bentonite as a
3 liner material at waste sites. When the dry density is above 1.8 kg/dm^3 , almost all the porosity
4 resides in the interlayers of Na-montmorillonite. Since anions are excluded from the
5 interlayers, the anion-accessible porosity becomes zero, and anion-diffusion is minimal
6 (Bourg et al., 2003).

7 Second, the number of stacks in the c -direction has considerable influence on the
8 interlayer porosity, with interlayer porosity increasing with n_c and reaching the maximum
9 when $n_c \approx 25$. The interlayer porosity halves with n_c when n_c is smaller than 3, and becomes
10 zero for $n_c = 1$.

11

12 **3.3. *Electrostatic double layer***

13

14 *3.3.1 MGC model vs. Donnan approximation*

15

16 An excess of cations and a deficit of anions in the electrostatic double layer neutralize the
17 charge at the outer surface of the montmorillonite. In a simple 1:1 electrolyte such as NaCl,
18 the extent of anion deficit is adequately described as a function of the distance from the
19 surface with the MGC model as demonstrated by (i) Monte Carlo and molecular dynamics
20 simulations (Carnie and Torrie, 1984; Wang et al., 2007; Tournassat et al., 2009) and (ii) by
21 comparison with experimental data over a wide range of NaCl concentrations (Sposito, 1992).

22 As a consequence, it is taken here as the reference model for anion exclusion estimation. Note
23 that these statements are true for ionic strength not exceeding 0.1. Nonetheless, we used them
24 as an approximation for higher ionic strengths.

1 In this model, the concentration $c(x)_i$ of a species i at a distance $x > 0$ from the surface, where
 2 $x = 0$ is the position of minimum approach of the ion (for example, $a = 0.184$ nm for
 3 chloride), is given by:

$$c(x)_i = c_{free,i} \exp\left(\frac{-z_i F \psi(x)}{RT}\right) \quad \text{Equation 10}$$

5
 6 where c_{free} is the concentration in free porewater (mol/L), z_i is the charge number (-), F is the
 7 Faraday constant (96485 C mol⁻¹), $\psi(x)$ is the electrostatic potential (V) at a distance x from
 8 the surface, R is the gas constant (8.134 J mol⁻¹ K⁻¹), and T is the temperature (K). The
 9 electrostatic potential is given by the combination of the following equations:

$$\frac{F\psi(x)}{RT} = 4 \times \operatorname{arctanh}\left[\tanh\left(\frac{F\psi(0)}{4RT}\right) \times \exp(-\kappa(x))\right] \quad \text{Equation 11}$$

$$\kappa = \sqrt{\frac{2F^2 1000c_{free,i}}{\mu_w RT}} \quad \text{Equation 12}$$

$$\frac{F\psi(0)}{2RT} = -\operatorname{arc\,sinh}\left(\frac{|\sigma|}{8\mu_w RTc_{free,i}}\right) \quad \text{Equation 13}$$

10
 11 where κ is the inverse of the debye length (m⁻¹), σ is the surface charge (C m⁻²) and μ_w the
 12 permittivity of water (6.93 10⁻¹⁰ F/m at 25 °C).

13 Equation 10 to Equation 13 allow calculation of a total chloride exclusion distance from the
 14 surface according to (Sposito, 2004):

$$d_{exc} - a = \lim_{x \rightarrow \infty} \int_a^x \left(1 - \frac{c_{Cl}(x')}{c_{free}}\right) dx' = \frac{2}{\kappa} \left(1 - \exp\left[-\frac{F|\psi(a)|}{2RT}\right]\right) \quad \text{Equation 14}$$

16

1 However, this binary representation (absence or presence of chloride, Figure 3) is not very
 2 representative of the system since the EDL is not completely devoid of anions. Alternatively,
 3 the exponential distribution of the ions in the EDL can be averaged over a Donnan porespace,
 4 (Donnan and Guggenheim, 1932; Leroy et al., 2006; Appelo and Wersin, 2007):

$$c_{D,i} = c_{free,i} \exp\left(\frac{-z_i F \psi_D}{RT}\right) \quad \text{Equation 15}$$

6
 7 where c_D is the concentration in the Donnan porespace (mol/L) and ψ_D is the Donnan
 8 potential (V). As an approximation, concentrations are used instead of activities in Equation
 9 15 (Appelo and Wersin, 2007; Birgersson and Karnland, 2009). The ions in the Donnan
 10 porespace balance the charge from the surface:

$$\sum_i c_{D,i} + q = 0 \quad \text{Equation 16}$$

12
 13 where q is the surface charge (mol_c/L).
 14 If the free porewater contains only $c_{Na^+} = c_{Cl^-} = c_{free}$, the Donnan potential can be solved
 15 combining Equation 15 and Equation 16:

$$c_{free} (B - B^{-1}) + q = 0 \quad \text{Equation 17}$$

17
 18 where $B = \exp\left(\frac{z_i F \psi_D}{RT}\right)$. The Cl⁻ concentration in the Donnan pore is then:

19

$$c_{D,Cl^-} = \frac{c_{free,Cl^-}}{B} = \frac{2c_{free}^2}{-q + \sqrt{q^2 + 4c_{free}^2}} \quad \text{Equation 18}$$

1
2 and the anion accessible porosity (ε_{an}) becomes:

$$\varepsilon_{an} = \varepsilon_{free} + \frac{\varepsilon_D c_{D,Cl^-}}{c_{free}} \quad \text{Equation 19}$$

4
5 where ε_{free} is the “free” porosity.

6 For solving Equation 18, the surface charge concentration q must be expressed as a function
7 of the montmorillonite’s external surface area and the thickness of the Donnan porespace (d_D ,
8 see Figure 3), which must be selected. The thickness can be set to a multiple of Debye lengths
9 (for example $d_D = 2$ Debye lengths, similar to the total anion exclusion distance given by
10 MGC), or B can be kept fixed, and d_D calculated from:

$$d_D = \frac{10^6 \text{ CEC} / n_c}{A_{ext} c_{free} \left(B - \frac{1}{B} \right)} \quad \text{Equation 20}$$

12
13 where d_D is in m. The resulting d_D ’s can be expressed in terms of Cl^- free d_{exc}^* ’s

$$d_{exc}^* - a = d_D \left(1 - \frac{c_{D,Cl^-}}{c_{free,Cl^-}} \right) = d_D \left(1 - \frac{1}{B} \right) \quad \text{Equation 21}$$

15 Comparing Equation 14 and Equation 21 shows that, if d_D is set equal to $2/\kappa$ in Equation 20
16 the same Cl^- free width will be calculated by the Gouy-Chapman and the Donnan equations
17 since the same surface charge is compensated. In this case, the potential at the start of the

1 *EDL* is twice the average potential in the Donnan volume. Anion-free thicknesses for the three
 2 models are presented in Figure 5 as a function of the NaCl concentration in the free solution.
 3 These thicknesses are limited by the maximum available thickness in the bentonite, shown by
 4 lines for three bentonite densities. For example, at $c_{free} = 0.01$ eq/L, the Gouy-Chapman
 5 thickness is 5.92 nm, which is also the maximum available when $\rho_{bent} = 1.1$ kg/L.
 6 Accordingly, at this ionic strength, the *EDL*'s overlap strongly, and the Gouy-Chapman
 7 formulas for truncated double layers must be applied (Goncalves et al., 2007). In the Donnan
 8 model with fixed $d_D = 2/\kappa$, $B = 17.8$ at this point, and the anion accessible porosity amounts to
 9 0.024. If, in the other option, B is fixed to a higher value, for example, $B = 30$ in Figure 5, the
 10 value of d_{exc}^* is 3.6 nm, and the anion-accessible porosity becomes 0.18. However, also in this
 11 case, the anion accessible porosity will become very small when ρ_{bent} is further increased to
 12 about 1.3 kg/L. The best option for estimating the Cl^- accessible porosity, and thus, the
 13 distribution of the porosities, must be verified against experimental data.

15 3.3.2 Stern layer charge compensation effect

16
 17 The above calculations were performed considering that the whole surface charge is
 18 compensated in the diffuse layer. Part of this charge is however compensated in the Stern
 19 layer in the first hydration layer at the mineral surface. Stern layer charge screening can be
 20 modelled by considering the reaction (Appelo et al., 2010):



22 where Su^- is a charged site at the surface. The corresponding fraction of charge that is
 23 compensated by Na in the Stern layer can be calculated with the diffuse layer model
 24 (Dzombak and Morel, 1990) or triple layer models (TLM) (Leroy et al., 2006). The TLM's
 25 have in common that the anion exclusion distance at the surface is given by the width of the

1 Stern layer, where anions are totally excluded, plus the anion exclusion distance obtained
2 from Equation 14 with potential terms corresponding to the potential of the head-end of the
3 diffuse layer (ψ_d in the TLM notation) instead of the potential at the clay surface. The width
4 of Stern layer will be about one to three water layers. However, complete anion exclusion
5 from this volume is questionable. For instance, molecular dynamics calculation shows that Cl⁻
6 can approach the clay surface closer than the second layer of adsorbed water (Marry et al.,
7 2008; Tournassat et al., 2009). Equation 14 shows that the anion exclusion distance depends
8 on the value of the potential that in turn depends on the affinity of Na for the surface (log
9 K_{NaSu} in reaction 19). Figure 4 shows clearly that, unless more than 80% of the charge is
10 compensated in the Stern layer, there is little effect of charge compensation on the anion
11 exclusion distance. Such a high charge compensation is not reported in the literature for NaCl
12 systems but may be attained when divalent cations are present (Leroy and Revil, 2004; Leroy
13 et al., 2007). As a consequence, this charge compensation effect will not be taken into account
14 in the following in order to keep the model as simple as possible.

15 **4. Initial water content and impurities**

16 The fraction of impurities can be obtained by mineralogical analysis and calculating their
17 mean density. Based on Madsen (1998) and Komine (2004), Bourg (2004) estimated the
18 density of impurities to be $2.82 \pm 0.58 \text{ kg/dm}^3$. This estimated density is rather high for quartz
19 and feldspar, which are probably the major impurities and large uncertainty on the value
20 prevents accurate estimation of impurities content. Densities can be estimated also from the
21 experiments of Van Loon et al. (2007), who reported water-uptake in Volclay-bentonite,
22 providing the total porespace for a given weight of bentonite. The (overall) bentonite density
23 in these experiments is $2.8 \pm 0.2 \text{ kg/dm}^3$. For a montmorillonite crystal density of 2.84 kg/dm^3
24 that was calculated before, and $r_{imp}=29\%$ impurities, the density of the impurities follows as

1 $\rho_{imp}=2.68\pm 0.30$ kg/dm³. The mean value is still higher than the density of quartz and feldspar,
 2 but Volclay contains 6% chlorite/smectite that may have a higher density due to its iron
 3 content. Moreover, the associated uncertainty remains large. Nevertheless, the values given
 4 above were used to recalculate the bentonite densities of Van Loon et al. (2007) to
 5 montmorillonite densities. The same values were applied as well to the MX80 bentonite used
 6 by Muurinen et al. (1989; 2004; 2007) and Molera et al. (2003), but with a 25% impurity
 7 content. The initial water content of bentonite dried at room temperature represents
 8 approximately $r_{water} = 10\%$ of the bentonite weight in the experiment of Van Loon et al., 2007
 9 ($r_{water} = 0\%$ for other literature data). This mass of water was also taken into account for this
 10 series of data to recalculate bentonite dry densities to montmorillonite partial dry densities
 11 ($\rho_{bd,mm}$) according to:

$$\rho_{bd,mm} = \frac{\rho_{bent}(1-r_{water})(1-r_{imp})}{1-r_{imp}\frac{\rho_{bent}}{\rho_{imp}}} \quad \text{Equation 23}$$

13
 14 where ρ_{bent} is the mass of bentonite in one dm³ (*i.e.* bentonite dry density).
 15 Anion accessible porosity measurements (ε_{an}^{meas}) were also normalized (ε_{an}^{norm}) to the bulk
 16 dry montmorillonite volume according to:

$$\varepsilon_{an}^{norm} = \varepsilon_{an}^{meas} \times \frac{1}{1-r_{imp}\frac{\rho_{bent}}{\rho_{imp}}} \quad \text{Equation 24}$$

18

1 Some experimental points were discarded. The reasons for this data selection, together with
2 the tabulated data, are given in Appendix A. In the following, all calculations are performed
3 relative to bulk dry montmorillonite densities and volumes.

4 Scatter in the experimental data cannot be avoided despite the data normalization and
5 selection procedures because the anion accessible porosity of a bentonite sample may depend
6 on the applied measurement procedure (Van Loon et al., 2007) and the sample pre-treatment
7 (Muurinen et al., 2007). For this reason, no attempt was made to calculate a mean porosity
8 value and an error band from data given for identical physical and chemical conditions.
9 Rather, the variability of the measured values is discussed in the light of the proposed models.

10

11 **5. Models for anion exclusion**

12 **5.1. Donnan porespace models**

13 Birgersson and Karnland (2009) lumped the whole porespace of bentonite into a
14 Donnan volume that was assigned the full charge of montmorillonite, thus $\varepsilon_{free} = \varepsilon_{IL} = 0$. The
15 results of this model are shown in Figure 6 (dashed black lines) and show a good agreement
16 (for such a simple model; SSD (sum of squared differences) = 1.89) with experimental
17 numbers for densities above 1.2 kg/dm³. For lower densities, the model underestimates the
18 anion accessible porosity. According to the discussion in section 3.2.1, this result is logical
19 because d_D is far higher than two Debye lengths at low densities. The model can be corrected
20 by setting $d_D = 2 \kappa^{-1}$. However, this correction does not improve the fit of data at densities
21 above 0.5 kg/dm³ (not shown).

22

23 The model can be improved by incorporating a second Donnan volume for the interlayer
24 porosity in the model, but still taking $\varepsilon_{free} = 0$ (Muurinen et al., 2007). Muurinen et al.

1 allocated the volumes as a function of the interlayer spacing (letting it decrease linearly with
2 bentonite density) and the internal and external surface areas, taking either a constant stacking
3 number $n_c \approx 31$, or a stacking number that decreases from $n_c = 40$ at 1.8 kg/dm^3 to $n_c = 4$ at
4 0.5 kg/dm^3 . By associating the surface area and the Donnan volumes, the charge is also
5 apportioned between the two volumes (interlayer and external). Muurinen et al. (2007) argued
6 that the two different ways of distributing the surface areas over the two Donnan volumes
7 should be related to bentonite preparation, and showed that surface area and its distribution
8 over the two Donnan volumes significantly influences the results. This model is successful in
9 describing the data but is questionable in that Cl^- is assigned to the interlayer space even at the
10 highest bentonite compaction where montmorillonite is into the form of a 2-layer hydrate.

12 ***5.2. Anion-free interlayer models***

13
14 The approach of Muurinen et al. (2007) was adapted assuming that the interlayer
15 porosity was devoid of anions (Rotenberg et al., 2007) and by subdividing the external
16 porespace into a Donnan volume and a free fraction. The internal porosity was calculated as
17 noted previously (with Equation 5 and Equation 8) and subtracted from the total porosity. In a
18 first calculation, the free part of the porosity was set to zero (model 1), *i.e.* the Donnan
19 volume occupies the whole external porosity. The fitted n_c value is 8.4 with SSD value of
20 0.74. The decrease of SSD indicates the better fit of the data than Birgersson and Karnland's
21 model (SSD = 1.89). However, this statement must be moderated by a more thorough
22 inspection of the data/model agreement. Figure 6, red full lines, shows that data at low
23 montmorillonite dry density values are now quite well reproduced, but data at high density are
24 ill-predicted for low ionic strength, where calculated anion accessible porosities go to zero or

1 to very small numbers. Also, the fitted stacking number n_c is higher than observed (Pusch,
2 2001; Melkior et al., 2009).

3 Model 1 can be changed slightly by considering that the Donnan volume should be
4 limited to two Debye lengths from the montmorillonite surface (section 3.2). Accordingly, the
5 Donnan volume was limited to two Debye lengths and the remaining porespace was
6 considered free porewater with the Cl^- concentration of the external solution. If the Donnan
7 porespace was larger than the available porespace, it was reduced to that part and free
8 porewater was zero. The results of this model 2 are shown on Figure 6 (red dash dotted lines).
9 The fitted n_c value is 2.48, now in agreement with observations, but SSD increased to 0.89.
10 For ionic strength below 0.1, agreement between data and model is better than with model 1
11 at high montmorillonite density values, whereas it is less satisfactory at low density values.
12 Note that the data at ionic strengths above 0.3 are very well reproduced by all of the models,
13 and that models which consider complete anion exclusion from the interlayer space reproduce
14 the data better than Birgersson and Karnland's model.

15 A conceptual problem may arise from the distinction between (i) the interlayer pore
16 space, where complete anion exclusion occurs, and (ii) the Donnan volume where anions have
17 access, in cases where the distance between two adjacent surfaces in the Donnan + free
18 volume (d_{pore}) is similar to, or smaller than, the distance between two adjacent surfaces in the
19 3WL interlayer space (0.94 nm). Now, d_{pore} can be approximated by:

$$d_{pore} = \frac{V_{ext}}{0.5 \times S_{ext}} \text{ (m)} \quad \text{Equation 25}$$

21

22 where V_{ext} is the pore volume minus the interlayer volume:

$$V_{ext} = V_{tot} \times \left(1 - \frac{10^6 \times \frac{ssa}{2} \times \rho_{bd,mm} \times (n_c - 1) \times h_{int}}{n_c} - \frac{\rho_{bd,mm}}{\rho_{mm}} \right) \quad (\text{m}^3) \quad \text{Equation 26}$$

1
2 And S_{ext} is the external surface area of montmorillonite:

$$S_{ext} = V_{tot} \times \frac{10^6 \times ssa \times \rho_{bd,mm}}{n_c} \quad (\text{m}^2) \quad \text{Equation 27}$$

4 Combining Equation 25 to Equation 27:

$$d_{pore} = 2 \times \frac{n_c \left(1 - \frac{\rho_{bd,mm}}{\rho_{mm}} \right) - 10^6 \times \frac{ssa}{2} \times \rho_{bd,mm} \times (n_c - 1) \times h_{int}}{10^6 \times ssa \times \rho_{bd,mm}} \quad (\text{m}) \quad \text{Equation 28}$$

5
6
7 Figure 7 shows that the condition $d_{pore} > 0.94$ nm is true only at montmorillonite bulk
8 dry densities below 1.6 kg/dm^3 . However, Equation 28 does not account for the possibly
9 larger pores that exist in the random three-dimensional arrangement of the crystals.

10 In order to explain anion accessibility (and diffusion) at high montmorillonite bulk densities
11 (chloride diffusion was measured at $\rho_{bd,mm}$ up to 1.8 kg/dm^3 , Kozaki et al., 1998b) we must
12 assume that anions have access to interlayer spaces and to pores of similar dimensions at high
13 montmorillonite density values ($> 1.6\text{-}1.7 \text{ kg/dm}^3$) or that clay platelets are re-arranged at
14 high montmorillonite density to form pores having dimensions larger than interlayer spaces.
15 This last hypothesis is explored here.

16 Looking at Equation 28 (and Figure 7) shows that an increase of d_{pore} at a given density
17 and NaCl concentration can only be achieved by an increase in n_c . Direct observations of Na-
18 montmorillonite compacted samples, e.g. by transmission electronic microscopy, show that n_c

1 ranges from 3-7 (Pusch, 2001; Melkior et al., 2009). Micrographs also show that the
2 microstructure is not homogeneous, but characterized by dense and less compact parts, the
3 latter having the largest pores in the material. It is likely that turbostratic arrangements occur
4 in the densest parts, where distances between adjacent surfaces can be of the same order as
5 interlayer spacing. At very high densities the structure might collapse altogether. Figure 8
6 depicts, very schematically, this microstructure.

7 We hypothesize that the clay TOT layers rearrange as a function of compaction and
8 ionic strength, keeping some pores with a minimum d_{pore_min} (model 3). Thus, the stacking
9 number n'_c may increase above n_c to include the contribution of turbostratic arrangements
10 even at low compaction where no true interlayer can be probed by XRD (“interlayer-like”
11 water). This stacking number was calculated by stepwise increasing n'_c from a minimal value
12 in case d_{pore} was smaller than d_{pore_min} for a given montmorillonite density and NaCl
13 concentration. n'_c was limited to $n'_{c_max} = 30$, corresponding to an external total surface area
14 of 25 m²/g, commensurable with the BET surface area of dry MX80 montmorillonite (Wanner
15 et al., 1994). Fitted n'_{c_min} value was 1.4, in agreement with montmorillonite tactoid size in
16 suspensions (Sposito, 1992), and fitted d_{pore_min} value was 5.5 Debye lengths (SSD = 0.65,
17 Figure 6). Most of the experimental data could be very satisfactorily reproduced by this
18 model, but it will be noted that it uses one more variable (d_{pore_min}) than the previous models.
19 Only data obtained at montmorillonite dry bulk densities higher than 1.6 kg/dm³ could not be
20 satisfactorily reproduced because n'_{c_max} was reached at these densities and the minimum pore
21 size could not be attained as a result.

22 This model would require further reduction of the interlayer space (2WL → 1WL) to
23 explain experimental results at the highest montmorillonite dry densities or alternatively,
24 interlayer water density different from 1 kg dm⁻³ should be considered (or a combination of
25 the two phenomena). There is not much evidence of this 2WL → 1WL transition in the

1 literature. González Sánchez et al. (2008) reports d-spacing of 14.66 Å for pure
 2 montmorillonite material at dry bulk densities of 1.9 kg/dm³. This value is significantly lower
 3 than the expected value for a 2WL interlayer space (~15.6 Å) but still higher than the
 4 expected value for a 1 WL interlayer (~12 Å). Van Loon et al. (2007) demonstrated that,
 5 when packed at high density, montmorillonite plugs exhibit an inhomogeneous density
 6 profile, with de-compacted regions near the external filters (1-2 mm on each side of a 1 cm
 7 plug). Given the penetration depth of X-rays in XRD measurements (order of magnitude = 1
 8 µm), these de-compacted regions would be dominant in the XRD signal and, therefore, the
 9 minimum montmorillonite dry density for the 2WL → 1WL transition is perhaps
 10 overestimated. If present, turbostratic arrangement having “interlayer like” domains with
 11 1WL size would not be probed either. As a consequence, we surmised that 1 WL domains are
 12 present at high montmorillonite dry bulk density and reduced, in a final model 4, the
 13 interlayer thickness if $n'_c = n'_{c_max}$ and $d_{pore} < d_{pore_min}$, with the constraint that the interlayer
 14 thickness should remain larger than h_{int}^{1WL} (~0.31 nm).

15 Figure 6 shows that such a transition (model 4) explains the observed anion porosity at
 16 high montmorillonite dry bulk density without needing to invoke Cl access to interlayer
 17 domains. The fit to the data is similar to that of the previous model 3 (SSD = 0.67). Model 3
 18 tends to underestimate anion accessible porosity at high montmorillonite densities while
 19 model 4 tends to overestimate it. Models 3 and 4 are in agreement with the observation of an
 20 effect of bentonite preparation on the measured anion accessible porosity value (Muurinen et
 21 al., 2007), this effect being incorporated in the d_{pore_min} value that should be very dependent on
 22 the initial spatial organization of TOT layers, and thus on the bentonite preparation (Muurinen
 23 et al., 2007) and the experimental conditions (Van Loon et al., 2007). It is of interest to
 24 consider the variation of d_{pore_min} when taken as variable for each individual measurement
 25 (Figure 9). Figure 9 shows also that at 0.1 ionic strength, 85% of 52 available data are

1 adequately described with a d_{pore_min} value comprised between 0.5 and 2 times the averaged
2 value (5.5 Debye lengths). At 0.01 ionic strength, 75% of 20 available data are in the same
3 interval.

4 The average value of d_{pore_min} can be used to predict anion accessible porosity as a
5 function of ionic strength and montmorillonite bulk density. The model can be further tested
6 on chloride accessible porosity data measured in pure montmorillonite (no impurity) samples.
7 Unfortunately very few data are available in which both porosity and ionic strength are
8 reported. The only one we found is the study by Glaus et al. (2010). In this study, data were
9 obtained at a single montmorillonite dry density of 1900 kg/dm³. For such high dry density,
10 the question whether the 2WL → 1WL transition occurs is crucial, and we stand at the limit
11 of the proposed approach. Models 1, 2 and 3 (Table 1) underestimate the measured anion
12 accessible porosity values for all ionic strengths. Considering the above model 4 at 0.1 mol L⁻¹
13 NaCl, the model predicts an accessible porosity of 0.043 (with $n'_c = 30$) while measured
14 values amounts to 0.019. At higher reported ionic strength measured and predicted porosity
15 values are respectively 0.036 vs. 0.03 ($I = 0.5$, $n'_c = 30$), 0.05 vs. 0.024 ($I = 1$, $n'_c = 30$) and
16 0.067 vs. 0.019 ($I = 2$, $n'_c = 30$). Although the agreement is still satisfactory, the trend of
17 predicted accessible porosity values as a function of ionic strength is opposite to measured. It
18 may be that a 2WL → 1WL transition takes place as a function of compaction and ionic
19 strength.

20 **6. Conclusions**

21 Simple models are successful in reproducing trends in anion exclusion in bentonite as a
22 function of ionic strength in the external solution and montmorillonite bulk dry densities in
23 the bentonite. When the pore space is assumed homogeneous regarding electrostatic
24 properties (*i.e.* a Donnan porespace which occupies all of the pore space, Birgersson and
25 Karnland, 2009), the anion accessible porosity measurements can be adequately modelled at

1 high montmorillonite partial densities but not at low montmorillonite densities. Also, data at
2 high ionic strength are better reproduced than data at low ionic strength. Models that consider
3 a heterogeneous pore distribution (interlayer region devoid of anions is subtracted from the
4 total porespace) reproduce the data better at low montmorillonite density but underestimate
5 the anion accessible porosity at very high density ($> 1.6-1.7 \text{ kg/dm}^3$) and low ionic strengths
6 (< 0.1). It is likely that the clay microstructure changes in this case, with the external pore
7 space gaining electrostatic properties similar to those of the interlayer pore space, because the
8 tactoids are packed densely together. This presentation offers the best fit for measured anion
9 accessible porosities in bentonites over a wide range of conditions and is in agreement with
10 microscopic observations. However, in this model, the stacking number (n_c) is a variable that
11 remains to be related in a general sense to sample preparation and experimental conditions.

12

13 ***7. Acknowledgments***

14 This research has been co-funded by POSIVA (Finland), ANDRA (France) in the
15 framework of the BRGM-ANDRA scientific partnership and by the European Commission
16 (sixth and seventh EURATOM Framework Programme for nuclear research and training
17 activities, FUNMIG, FP6-516514 and CATCLAY, FP7 249624). Dr. Eric Oelkers, Associate
18 Editor, Dr. Martin Glaus and two anonymous referees are acknowledged for their constructive
19 comments on the manuscript.

20

21 ***8. Supporting Information Available***

22 Tabulation of selected data.

23 A C-program for calculating the model results plotted on Figure 6.

9. References

- Altmann, S., 2008. 'Geo'chemical research: A key building block for nuclear waste disposal safety cases. *J. Contam. Hydrol.* **102**, 174-179.
- ANDRA, 2005. Référentiel du comportement des radionucléides et des toxiques chimiques d'un stockage dans le Callovo-Oxfordien jusqu'à l'Homme. Dossier 2005 Argile. Agence Nationale pour la gestion des déchets radioactifs, Châtenay-Malabry, France.
- Appelo, C. A. J., Van Loon, L. R., and Wersin, P., 2010. Multicomponent diffusion of a suite of tracers (HTO, Cl, Br, I, Na, Sr, Cs) in a single sample of Opalinus Clay. *Geochim. Cosmochim. Acta* **74**, 1201-1219.
- Appelo, C. A. J. and Wersin, P., 2007. Multicomponent diffusion modeling in clay systems with application to the diffusion of tritium, iodide, and sodium in Opalinus clay. *Environ. Sci. Technol.* **41**, 5002-5007.
- Bérend, I., Cases, J. M., François, M., Uriot, J. P., Michot, L. J., Masion, A., and Thomas, F., 1995. Mechanism of adsorption and desorption of water vapour by homoionic montmorillonites: 2. the Li⁺, Na⁺, K⁺, Rb⁺ and Cs⁺ exchanged forms. *Clays Clay Miner.* **43**, 324-336.
- Birgersson, M. and Karnland, O., 2009. Ion equilibrium between montmorillonite interlayer space and an external solution-Consequences for diffusional transport. *Geochim. Cosmochim. Acta* **73**, 1908-1923.
- Bolt, G. H. and De Haan, F. A. M., 1982. *Soil Chemistry. B. Physico-Chemical Models.* Elsevier, Amsterdam/New York.
- Bolt, G. H. and Warkentin, B. P., 1958. The negative adsorption of anions by clay suspensions. *Kolloid Zeitschrift* **156**, 41-46.
- Bourg, I. C., 2004. Tracer diffusion of water and inorganic ions in compacted saturated sodium bentonite, University of California, Berkeley.
- Bourg, I. C., Bourg, A. C. M., and Sposito, G., 2003. Modeling diffusion and adsorption in compacted bentonite: a critical review. *J. Contam. Hydrol.* **61**, 293-302.
- Bourg, I. C., Sposito, G., and Bourg, A. C. M., 2006. Tracer diffusion in compacted, water-saturated bentonite. *Clay. Clay. Miner.* **54**, 363-374.
- Bourg, I. C., Sposito, G., and Bourg, A. C. M., 2007. Modeling cation diffusion in compacted water-saturated sodium bentonite at low ionic strength. *Environ. Sci. Technol.* **41**, 8118-8122.
- Bouyoucos, G. J., 1921. The concentration of the soil solution around the soil particles *Soil Sci.* **11**, 131-138.
- Bradbury, M. H. and Baeyens, B., 2003. Porewater chemistry in compacted re-saturated MX-80 bentonite. *J. Contam. Hydrol.* **61**, 329-338.
- Carnie, S. L. and Torrie, G. M., 1984. The statistical mechanics of the electrical double layer. *Adv. Chem. Phys.* **56**, 141-253.
- Cases, J. M., Bérend, I., Besson, G., François, M., Uriot, J.-P., Thomas, F., and Poirier, J. E., 1992. Mechanism of adsorption and desorption of water vapor by homoionic montmorillonite. 1. The sodium-exchanged form. *Langmuir* **8**, 2730-2739.
- Cases, J. M., Bérend, I., Besson, G., François, M., Uriot, J.-P., Thomas, F., and Poirier, J. E., 1995. Mechanism of adsorption and desorption of water vapor by homoionic montmorillonite. 2. The Li⁺, K⁺, Rb⁺ and Cs⁺-exchanged forms. *Clay. Clay. Miner.* **43**, 324-336.
- Cases, J. M., Bérend, I., François, M., Serekova, Uriot, J. P., Michot, L. J., and Thomas, F., 1997. Mechanism of adsorption and desorption of water vapour by homoionic

- 1 montmorillonite: 3. the Mg^{2+} , Ca^{2+} , Sr^{2+} and Ba^{2+} exchanged forms. *Clays Clay Miner.*
2 **45**, 8-22.
- 3 Chavez-Paez, M., dePablo, L., and dePablo, J. J., 2001. Monte Carlo simulations of Ca-
4 montmorillonite hydrates. *The Journal of Chemical Physics* **114**, 10948-10953.
- 5 Descostes, M., Blin, V., Bazer-Bachi, F., Meier, P., Grenut, B., Radwan, J., Schlegel, M. L.,
6 Buschaert, S., Coelho, D., and Tevissen, E., 2008. Diffusion of anionic species in
7 Callovo-Oxfordian argillites and Oxfordian limestones (Meuse/Haute-Marne, France).
8 *Appl. Geochem.* **23**, 655-677.
- 9 Donnan, E. G. and Guggenheim, E. A., 1932. Die genaue Thermodynamik der membran-
10 gleichgewichte. *Zeitschrift fuer Physikalische Chemie (Leipzig, Germany)* **162**, 346-
11 360.
- 12 Dzombak, D. A. and Morel, F. M. M., 1990. *Surface complexation modeling-Hydrous ferric*
13 *oxide*, New York.
- 14 Edwards, D. G., Posner, A. M., and Quirk, J. P., 1965. Repulsion of chloride ions by
15 negatively charged clay surfaces. Part 2.-Monovalent cation montmorillonites.
16 *Transactions of the Faraday Society* **61**, 2816-2819.
- 17 Edwards, D. G. and Quirk, J. P., 1962. Repulsion of chloride by montmorillonite. *Journal of*
18 *colloid science* **17**, 872-882.
- 19 Ferrage, E., Lanson, B., Michot, L. J., and Robert, J. L., 2010. Hydration Properties and
20 Interlayer Organization of Water and Ions in Synthetic Na-Smectite with Tetrahedral
21 Layer Charge. Part 1. Results from X-ray Diffraction Profile Modeling. *Journal of*
22 *Physical Chemistry C* **114**, 4515-4526.
- 23 Ferrage, E., Lanson, B., Sakharov, B. A., and Drits, V. A., 2005. Investigation of smectite
24 hydration properties by modeling experimental X-ray diffraction patterns: Part I.
25 Montmorillonite hydration properties. *Am. Mineral.* **90**, 1358-1374.
- 26 Ferrage, E., Lanson, B., Sakharov, B. A., Geoffroy, N., Jacquot, E., and Drits, V. A., 2007.
27 Investigation of dioctahedral smectite hydration properties by modeling of X-ray
28 diffraction profiles: Influence of layer charge and charge location. *Am. Mineral.* **92**,
29 1731-1743.
- 30 Glaus, M. A., Frick, S., Rosse, R., and Van Loon, L. R., 2010. Comparative study of tracer
31 diffusion of HTO, Na-22(+) and Cl-36(-) in compacted kaolinite, illite and
32 montmorillonite. *Geochim. Cosmochim. Acta* **74**, 1999-2010.
- 33 Goncalves, J., Rousseau-Gueutin, P., and Revil, A., 2007. Introducing interacting diffuse
34 layers in TLM calculations: A reappraisal of the influence of the pore size on the
35 swelling pressure and the osmotic efficiency of compacted bentonites. *J. Colloid*
36 *Interface Sci.* **316**, 92-99.
- 37 Gonzales-Sanchez, F., Van Loon, L. R., Gimmi, T., Jakob, A., Glaus, M. A., and Diamond, L.
38 W., 2008. Self-diffusion of water and its dependence on temperature and ionic
39 strength in highly compacted montmorillonite, illite and kaolinite. *Appl. Geochem.* **23**,
40 3840-3851.
- 41 Goto, T., Kozaki, T., and Sato, S., 2008. Effects of dry density and salinity on basal spacing
42 of compacted montmorillonite. *Fall Meeting of the Atomic Energy Society of Japan*
43 *Kochi University of Technology*.
- 44 Grambow, B., 2008. Mobile fission and activation products in nuclear waste disposal. *J.*
45 *Contam. Hydrol.* **102**, 180-186.
- 46 Karaborni, S., Smit, B., Heidug, W., Urai, J., and vanOort, E., 1996. The swelling of clays:
47 Molecular simulations of the hydration of montmorillonite. *Science* **271**, 1102-1104.
- 48 Komine, H., 2004. Simplified evaluation for swelling characteristics of bentonites. *Eng. Geol.*
49 **71**, 265-279.

- 1 Kozaki, T., Fujishima, A., Sato, S., and Ohashi, H., 1998a. Self-diffusion of sodium ions in
2 compacted montmorillonite. *Nucl. Technol.* **121**, 63-69.
- 3 Kozaki, T., Inada, K., Sato, S., and Ohashi, H., 2001. Diffusion mechanism of chloride ions in
4 sodium montmorillonite. *J. Contam. Hydrol.* **47**, 159-170.
- 5 Kozaki, T., Liu, J. H., and Sato, S., 2008. Diffusion mechanism of sodium ions in compacted
6 montmorillonite under different NaCl concentration. *Physics and Chemistry of the*
7 *Earth* **33**, 957-961.
- 8 Kozaki, T., Saito, N., Fujishima, A., Sato, S., and Ohashi, H., 1998b. Activation energy for
9 diffusion of chloride ions in compacted sodium montmorillonite. *J. Contam. Hydrol.*
10 **35**, 67-75.
- 11 Le Forestier, L., Muller, F., Villieras, F., and Pelletier, M., 2010. Textural and hydration
12 properties of a synthetic montmorillonite compared with a natural Na-exchanged clay
13 analogue. *Applied Clay Science* **48**, 18-25.
- 14 Leroy, P. and Revil, A., 2004. A triple-layer model of the surface electrochemical properties
15 of clay minerals. *J. Colloid Interface Sci.* **270**, 371-380.
- 16 Leroy, P., Revil, A., Altmann, S., and Tournassat, C., 2007. Modeling the composition of the
17 pore water in a clay-rock geological formation (Callovo-Oxfordian, France). *Geochim.*
18 *Cosmochim. Acta* **71**, 1087-1097.
- 19 Leroy, P., Revil, A., and Coelho, D., 2006. Diffusion of ionic species in bentonite. *J. Colloid*
20 *Interface Sci.* **296**, 248-255.
- 21 Liu, J., Yamada, H., Kozaki, T., Sato, S., and Ohashi, H., 2003. Effect of silica sand on
22 activation energy for diffusion of sodium ions in montmorillonite and silica sand
23 mixture. *J. Contam. Hydrol.* **61**, 85-93.
- 24 Madsen, F. T., 1998. Clay mineralogical investigations related to nuclear waste disposal. *Clay*
25 *Miner.* **33**, 109-129.
- 26 Marry, V., Rotenberg, B., and Turq, P., 2008. Structure and dynamics of water at a clay
27 surface from molecular dynamics simulation. *Phys. Chem. Chem. Phys.* **10**, 4802-
28 4813.
- 29 Marry, V., Turq, P., Cartailier, T., and Levesque, D., 2002. Microscopic simulation for
30 structure and dynamics of water and counterions in a monohydrated montmorillonite.
31 *J. Chem. Phys.* **117**, 3454-3463.
- 32 Melkior, T., Gaucher, E. C., Brouard, C., Yahiaoui, S., Thoby, D., Clinard, C., Ferrage, E.,
33 Guyonnet, D., Tournassat, C., and Coelho, D., 2009. Na⁺ and HTO diffusion in
34 compacted bentonite: Effect of surface chemistry and related texture. *J. Hydr.* **370**, 9-
35 20.
- 36 Molera, M., Eriksen, T., and Jansson, M., 2003. Anion diffusion pathways in bentonite clay
37 compacted to different dry densities. *Applied Clay Science* **23**, 69-76.
- 38 Muurinen, A., Karnland, O., and Lehtikoinen, J., 2004. Ion concentration caused by an
39 external solution into the porewater of compacted bentonite. *Phys. Chem. Earth.* **29**,
40 119-127.
- 41 Muurinen, A., Karnland, O., and Lehtikoinen, J., 2007. Effect of homogenization on the
42 microstructure and exclusion of chloride in compacted bentonite. *Phys. Chem. Earth.*
43 **32**, 485-490.
- 44 Muurinen, A., Penttilä-Hilthunen, P., and Uusheimo, K., 1989. Diffusion of chloride and
45 uranium in compacted sodium bentonite. In: Lutze, W. and Ewing, R. C. Eds.),
46 *Scientific basis for nuclear waste management XII, Mat. Res. Soc. Symp. Proc.*
47 *Materials Research Society, Pittsburgh, PA.*
- 48 NAGRA., 2002. Project Opalinus Clay. NAGRA, Wettingen, Switzerland.
- 49 Nykyri, M., Nordman, H., Löfman, J., Poteri, A., Marcos, N., and Hautojärvi, A., 2008.
50 Radionuclide Release and Transport – RNT-2008. POSIVA.

- 1 Ochs, M., Lothenbach, B., Wanner, H., Sato, H., and Mikazu, Y., 2001. An integrated
2 sorption-diffusion model for the calculation of consistent distribution and diffusion
3 coefficients in compacted bentonite. *J. Contam. Hydrol.* **47**, 283-296.
- 4 Perronnet, M., Villieras, F., Jullien, M., Razafitianamaharavo, A., Raynal, J., and Bonnin, D.,
5 2007. Towards a link between the energetic heterogeneities of the edge faces of
6 smectites and their stability in the context of metallic corrosion. *Geochim.*
7 *Cosmochim. Acta* **71**, 1463-1479.
- 8 Pusch, R., 2001. The microstructure of MX-80 clay with respect to its bulk physical
9 properties under different environmental conditions. SKB, TR-01-08.
- 10 Rotenberg, B., Marry, V., Vuilleumier, R., Malikova, N., Simon, C., and Turq, P., 2007.
11 Water and ions in clays: Unraveling the interlayer/micropore exchange using
12 molecular dynamics. *Geochim. Cosmochim. Acta* **71**, 5089-5101.
- 13 Schofield, R. K., 1947. Calculation of surface areas from measurements of negative
14 adsorption. *Nature* **160**.
- 15 Slade, P. G., Quirk, J. P., and Norrish, K., 1991. Crystalline swelling of smectite samples in
16 concentrated NaCl solutions in relation to layer charge. *Clay. Clay. Miner.* **39**, 234-
17 238.
- 18 Sposito, G., 1992. The diffuse-ion swarm near smectite particles suspended in 1:1 electrolyte
19 solutions: modified Gouy-Chapman theory and quasicrystal formation. In: Güven, N.
20 and Pollastro, R. M. Eds.), *Clay-water interface and its rheological implications*. Clay
21 minerals society.
- 22 Sposito, G., 2004. *The Surface Chemistry of Natural Particles*. Oxford University Press, New
23 York.
- 24 Tambach, T. J., Hensen, E. J. M., and Smit, B., 2004. Molecular simulations of swelling clay
25 minerals. *J. Phys. Chem. B* **108**, 7586-7596.
- 26 Tournassat, C., Chapron, Y., Leroy, P., Bizi, M., and Boulahya, F., 2009. Comparison of
27 molecular dynamics simulations with Triple Layer and modified Gouy-Chapman
28 models in a 0.1 M NaCl - montmorillonite system. *J. Colloid Interface Sci.* **339**, 533-
29 541.
- 30 Tournassat, C., Neaman, A., Villieras, F., Bosbach, D., and Charlet, L., 2003.
31 Nanomorphology of montmorillonite particles: Estimation of the clay edge sorption
32 site density by low-pressure gas adsorption and AFM observations. *Am. Mineral.* **88**,
33 1989-1995.
- 34 Van Loon, L. R., Glaus, M. A., and Müller, W., 2007. Anion exclusion effects in compacted
35 bentonites: Towards a better understanding of anion diffusion. *Appl. Geochem.* **22**,
36 2536-2552.
- 37 Wang, M., Liu, J., and Chen, S., 2007. Electric potential distribution in nanoscale
38 electroosmosis: from molecules to continuum. *Mol. Simul.* **33**, 1273-1277.
- 39 Wanner, H., Albinson, Y., Karnland, O., Wieland, E., Wersin, P., and Charlet, L., 1994. The
40 acid/base chemistry of montmorillonite. *Radiochim. Acta* **66/67**, 157-162.
- 41 Yokoyama, S., Kuroda, M., and Sato, T., 2005. Atomic force microscopy study of
42 montmorillonite dissolution under highly alkaline conditions. *Clay. Clay. Miner.* **53**,
43 147-154.
- 44 Young, D. A. and Smith, D. E., 2000. Simulations of clay mineral swelling and hydration:
45 Dependence upon interlayer ion size and charge. *J. Phys. Chem. B* **104**, 9163-9170.
46
47

1 Table 1. Summary of models
 2
 3

Model name	Type of model
Birgersson and Karnland	Single Donnan-type porosity
Model 1	Double porosity model with interlayer porosity devoid of anions. Fixed number of TOT layer in tactoids (n_c). Donnan volume occupying all non interlayer porosity.
Model 2	Double porosity model with interlayer devoid of anions Fixed number of TOT layer in tactoids. Donnan volume extending up to two Debye lengths from the montmorillonite surface if possible, else equal to the non interlayer porosity.
Model 3	Double porosity model with interlayer devoid of anions Variable number of TOT layer in tactoids from $n_{c_min} = 1.5$ to $n_{c_max} = 30$. n_c increases to maintain $d_{pore} > d_{pore_min}$ (5.5 Debye lengths). Donnan volume extending up to two Debye lengths from the montmorillonite surface if possible, else equal to the non interlayer porosity.
Model 4	Same as model 3 except that interlayer space can be reduced to 1 WL at high montmorillonite density to maintain $d_{pore} > d_{pore_min}$.

4
 5
 6

1
2
3
4
5
6
7
8
9
10
11
12
13
14
15
16
17
18
19
20
21
22
23
24
25
26
27
28
29
30
31
32
33
34
35
36
37
38
39
40
41
42

Figures captions

Figure 1. Schematic representation of “interlayer water”, “electrostatic double layer water” and “free water” in compacted bentonite (Modified from Bradbury and Baeyens, 2003).

Figure 2. Interlayer porosity as a function of Na-montmorillonite dry density, stacking number of TOT layers, and NaCl concentration in free porewater. Total specific surface area is 749 m²/g.

Figure 3. Anion exclusion in the EDL according to (i) MGC model (black curve), (ii) total anion exclusion distance (dashed red line on top figure), and (iii) Donnan approximation with a Donnan volume extending up to two Debye lengths from the surface position (blue line on bottom figure). NaCl concentration is 0.1 mol/L. Surface charge corresponds to the CEC (0.81 mol_c/kg) and total specific surface area (749 m²/g) of MX80.

Figure 4. Influence of the fraction of charge compensated by the Stern layer on the anion exclusion distance.

Figure 5. Thickness of the anion-free electrostatic double layer at the montmorillonite surface, calculated 1) by Gouy-Chapman (full line), 2) as a Donnan porespace of fixed width $d_D = 2/\kappa$ (circles), and 3) as a Donnan porespace with fixed $B = c_{free, Cl^-} / c_{D, Cl^-}$ (dashed line). The Donnan thickness is expressed in equivalent anion-free thickness with Equation 19. The lines marked by triangles denote the maximal available thickness for 3 bentonite bulk densities, after the interlayer water has been subtracted from the porespace. The interlayer water is calculated for montmorillonite with a specific surface area of 749 m²/g and a stacking number $n_c = 4.6$.

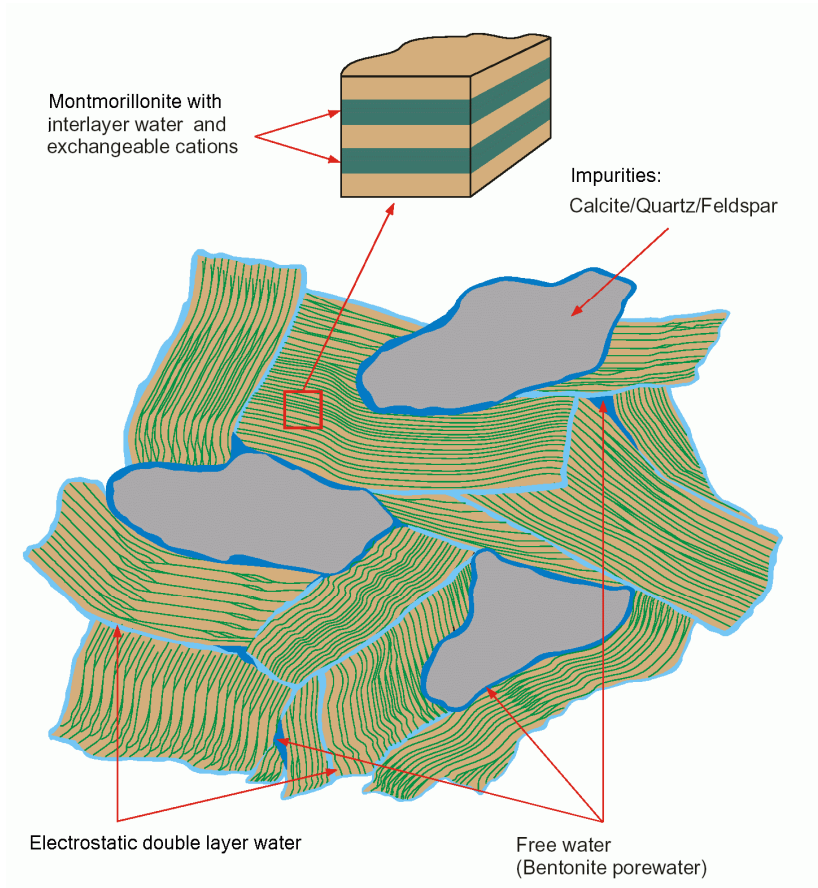
Figure 6. Anion accessible porosities in bentonite as a function of the dry density and the NaCl concentration in an external solution. The experiments are from Muurinen et al. (1989; 2004; 2007), Molera et al. (2003), and Van Loon et al. (2007). Data are corrected for impurity and water content. The black dashed lines are from a model with a single Donnan-type porosity (Birgersson and Karnland, 2009), full red lines are from the model 1 ($n_c = 8.4$, Donnan volume = non interlayer porosity), dash-dot red lines are from model 2 ($n_c = 2.48$, Donnan volume extending up to two debye lengths from the montmorillonite surface, if possible, else equal to the non interlayer porosity), dotted blue lines are from model 3 ($n'_{c_min} = 1.5$; $d_{pore_min} = 5.5 \kappa^{-1}$), full blue lines are from model 4 ($n'_{c_min} = 1.5$; $d_{pore_min} = 5.5 \kappa^{-1}$, $h_{intmin} = 0.33$ nm). In models 1 to 4, interlayer porosity is assumed Cl⁻-free and the external porespace is subdivided in a Donnan volume and (possibly) free porewater with the Cl⁻ concentration of the external solution. The crystallographic specific surface area is 749 m²/g.

Figure 7. Calculated poresize in bentonite as a function of density (d_{pore} Equation 25; plain lines for $c_{NaCl} = 0.01$ mol/L; dash-dotted lines for 1 mol/L) and the 3WL interlayer distance: above $\rho_{bd, mm} \approx 1.6$ kg/L the calculated pore diameter is smaller than the interlayer width.

Figure 8. Scheme of montmorillonite microstructure at high density.

Figure 8. Comparison between measured an modelled anion accessible porosity according to model 4 and a fitted minimum pore size. Corresponding pore sizes are given on the right figure where dash lines are representative of the minimum pore size value used in

1
2



3
4
5
6
7
8

Figure 1. Schematic representation of “interlayer water”, “electrostatic double layer water” and “free water” in compacted bentonite (Modified from Bradbury and Baeyens, 2003).

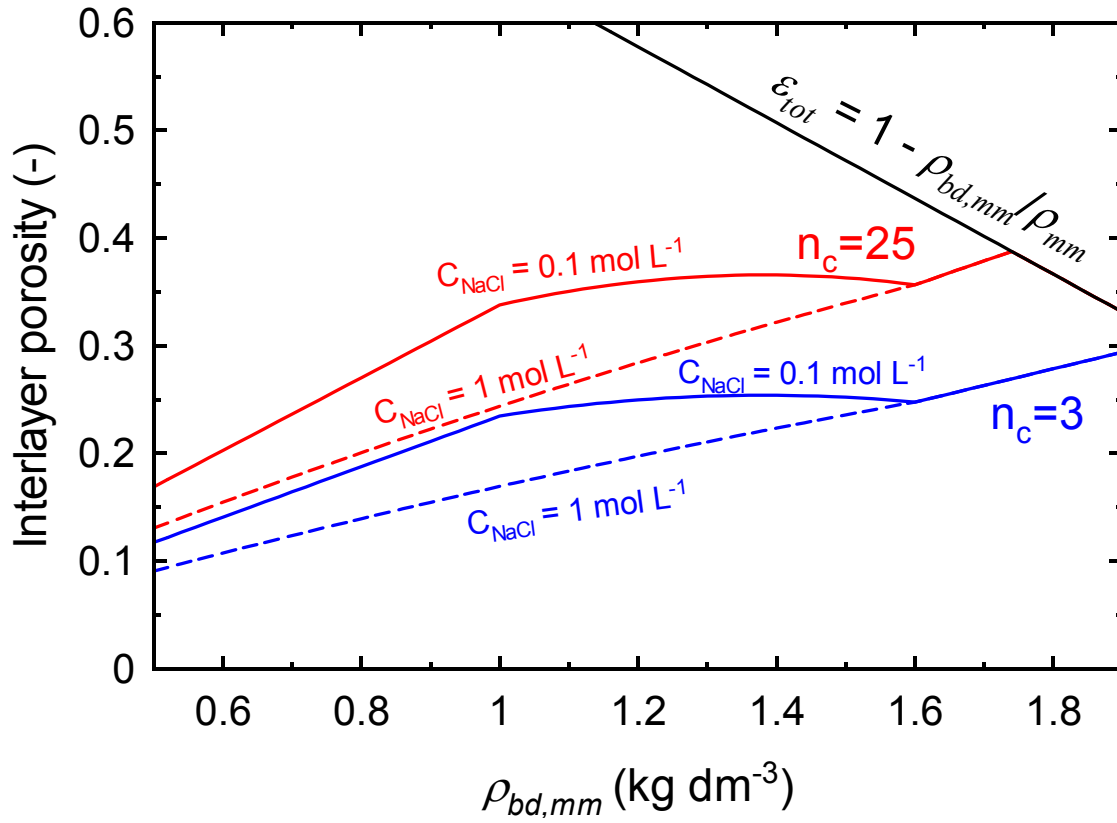
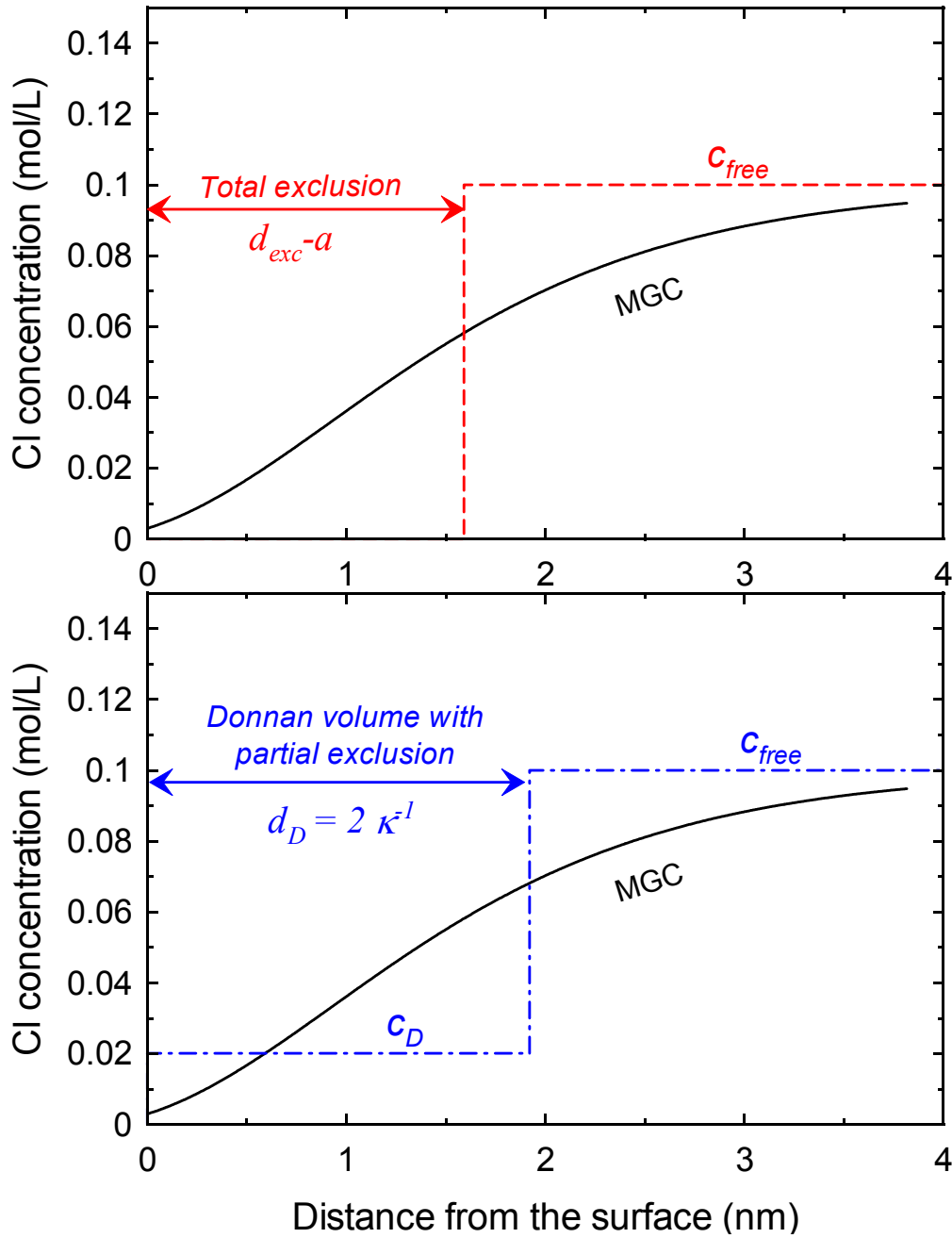
1
23
4
5
6
7

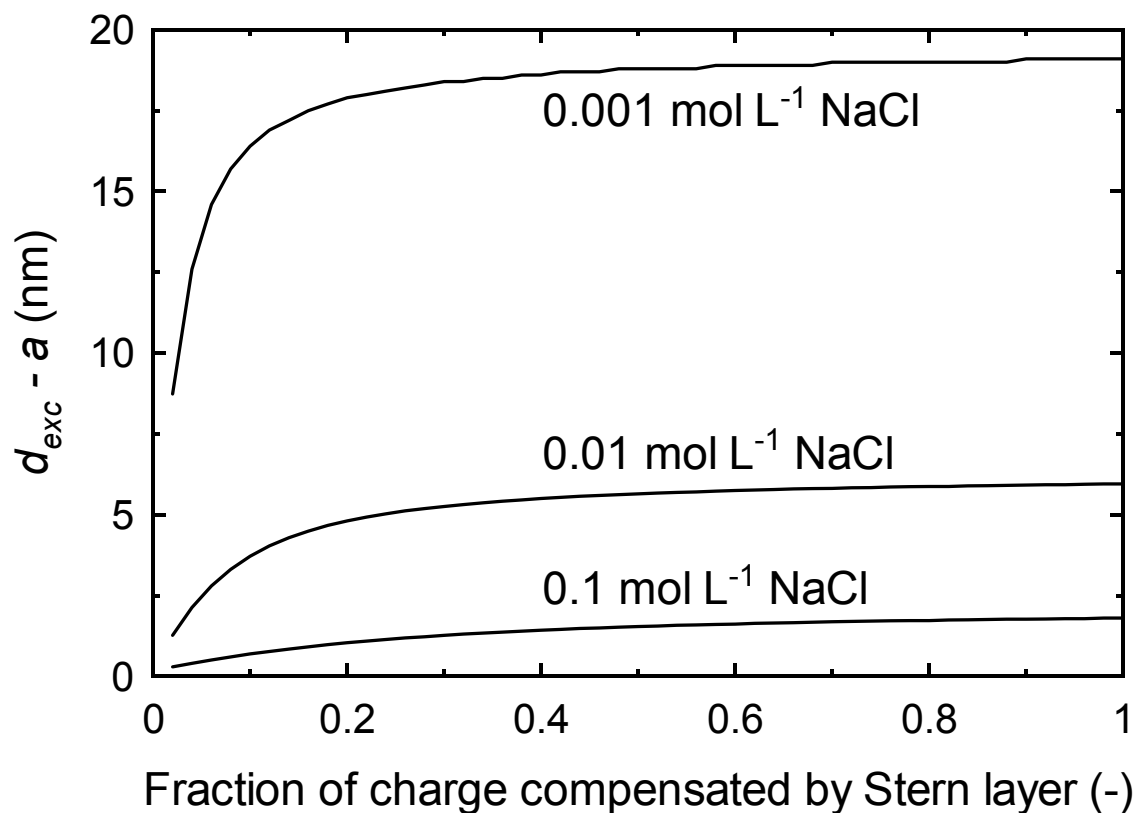
Figure 2. Interlayer porosity as a function of Na-montmorillonite dry density, stacking number of TOT layers, and NaCl concentration in free porewater. Total specific surface area is 749 m²/g.



1

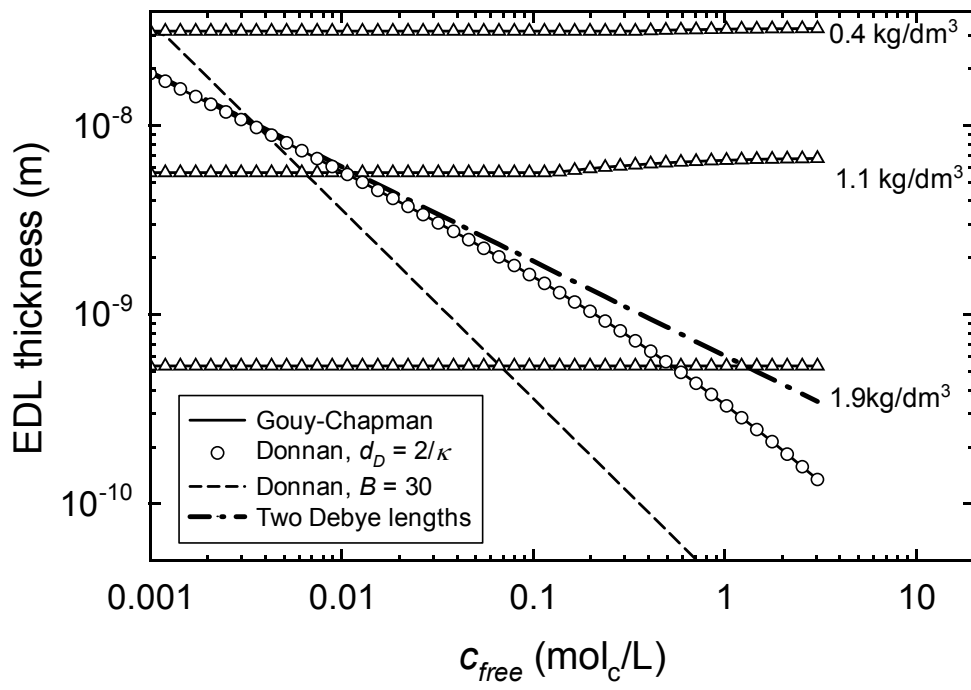
2

3 Figure 3. Anion exclusion in the EDL according to (i) MGC model (black curve), (ii) total
 4 anion exclusion distance (dashed red line on top figure), and (iii) Donnan approximation with
 5 a Donnan volume extending up to two Debye lengths from the surface position (blue line on
 6 bottom figure). NaCl concentration is 0.1 mol/L. Surface charge corresponds to the CEC
 7 (0.81 mol_e/kg) and total specific surface area (749 m²/g) of MX80.



1
2 Figure 4. Influence of the fraction of charge compensated by the Stern layer on the anion
3 exclusion distance.

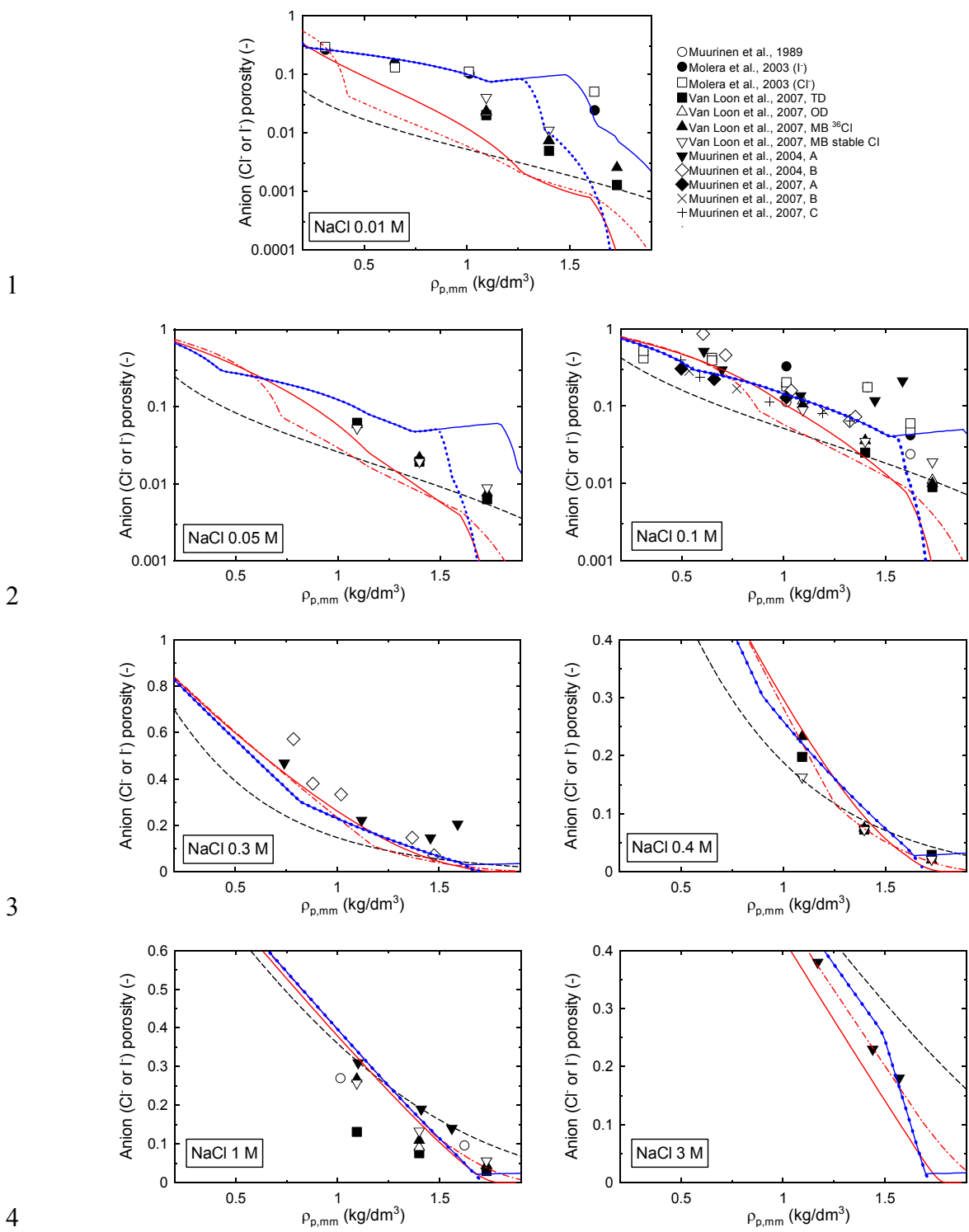
4
5

1
2

3

4 Figure 5. Thickness of the anion-free electrostatic double layer at the montmorillonite surface,
 5 calculated 1) by Gouy-Chapman (full line), 2) as a Donnan porespace of fixed width $d_D = 2/\kappa$
 6 (circles), and 3) as a Donnan porespace with fixed $B = c_{free, Cl^-} / c_{D, Cl^-}$ (dashed line). The
 7 Donnan thickness is expressed in equivalent anion-free thickness with Equation 21. The lines
 8 marked by triangles denote the maximal available thickness for 3 bentonite bulk densities,
 9 after the interlayer water has been subtracted from the porespace. The interlayer water is
 10 calculated for montmorillonite with a specific surface area of $749 \text{ m}^2/\text{g}$ and a stacking number
 11 $n_c = 4.6$.

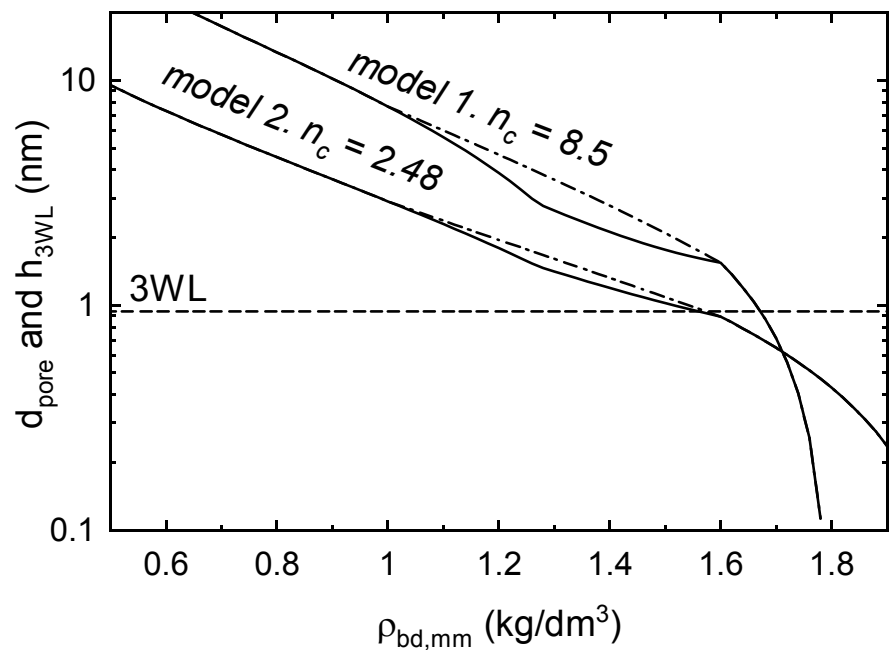
12



5 Figure 6. Anion accessible porosities in bentonite as a function of the dry density and the
 6 NaCl concentration in an external solution. The experiments are from Muurinen et al. (1989;
 7 2004; 2007), Molera et al. (2003), and Van Loon et al. (2007). Data are corrected for impurity
 8 and water content. The black dashed lines are from a model with a single Donnan-type
 9 porosity (Birgersson and Karnland, 2009), full red lines are from the model 1 ($n_c = 8.4$),

1 dash-dot red lines are from model 2 ($n_c = 2.48$), dotted blue lines are from model 3 ($n_{c_min} =$
2 1.5 ; $d_{pore_min} = 5.5 \text{ } \kappa^{-1}$), full blue lines are from model 4 ($n'_{c_min} = 1.5$; $d_{pore_min} = 5.5 \text{ } \kappa^{-1}$, h_{intmin}
3 $= 0.33 \text{ nm}$). Summary of models are given in Table 1. The crystallographic specific surface
4 area is $749 \text{ m}^2/\text{g}$.
5

1
2



3
4
5
6
7
8
9
10

Figure 7. Calculated poresize in bentonite as a function of density (d_{pore} Equation 28; plain lines for $c_{NaCl} = 0.01$ mol/L; dash-dotted lines for 1 mol/L) and the 3WL interlayer distance: above $\rho_{bd,mm} \approx 1.6$ kg/L the calculated pore diameter is smaller than the interlayer width.

1
2
3
4
5
6

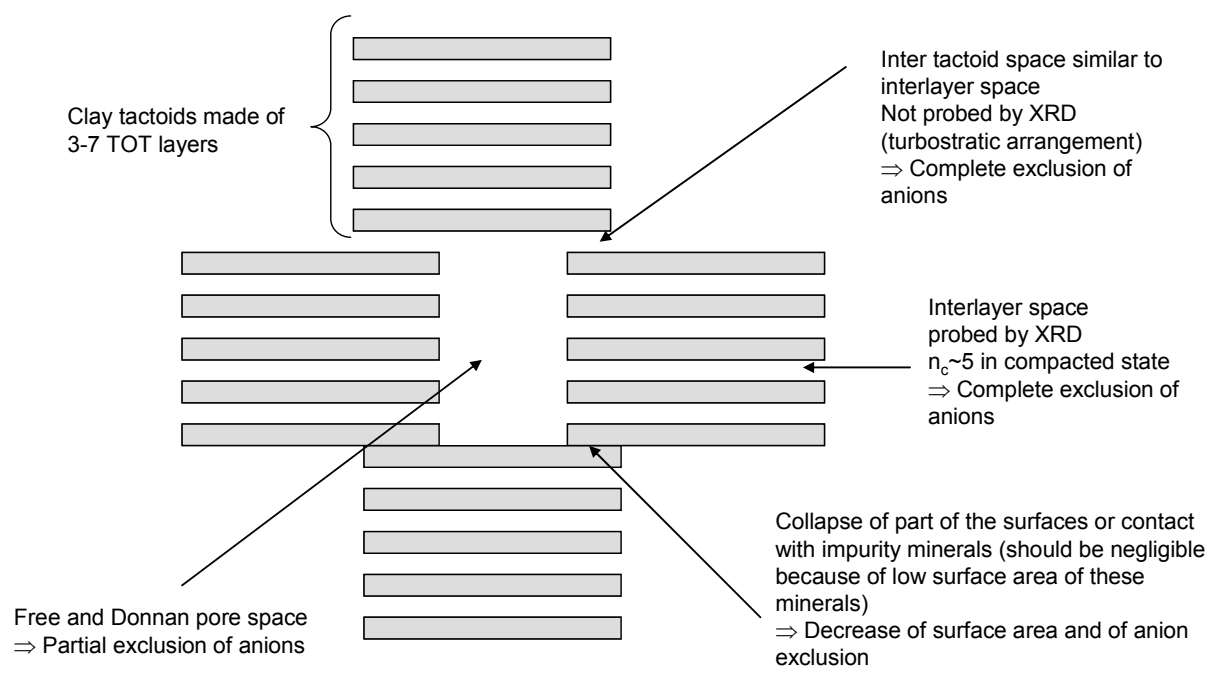
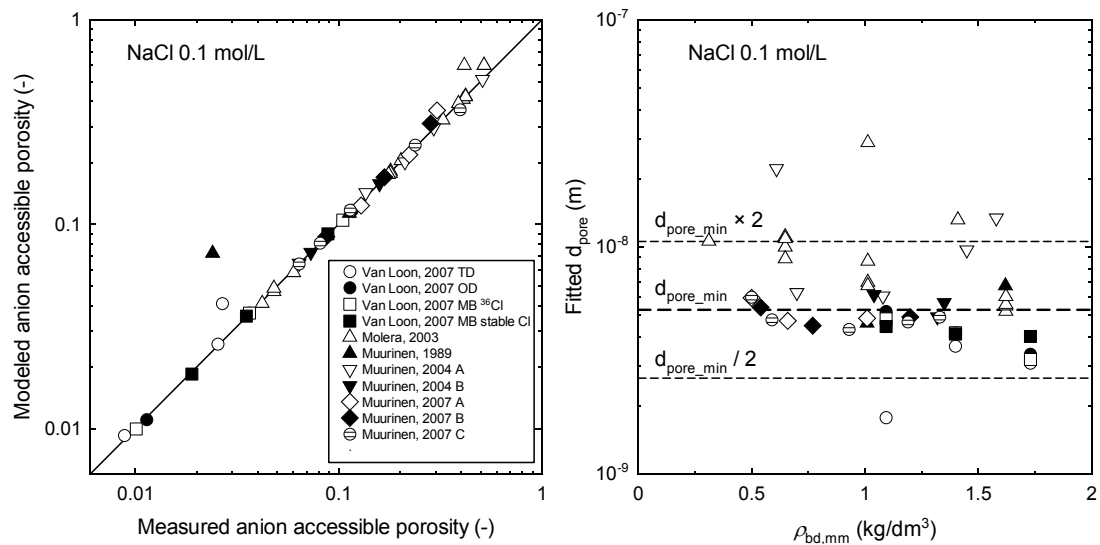
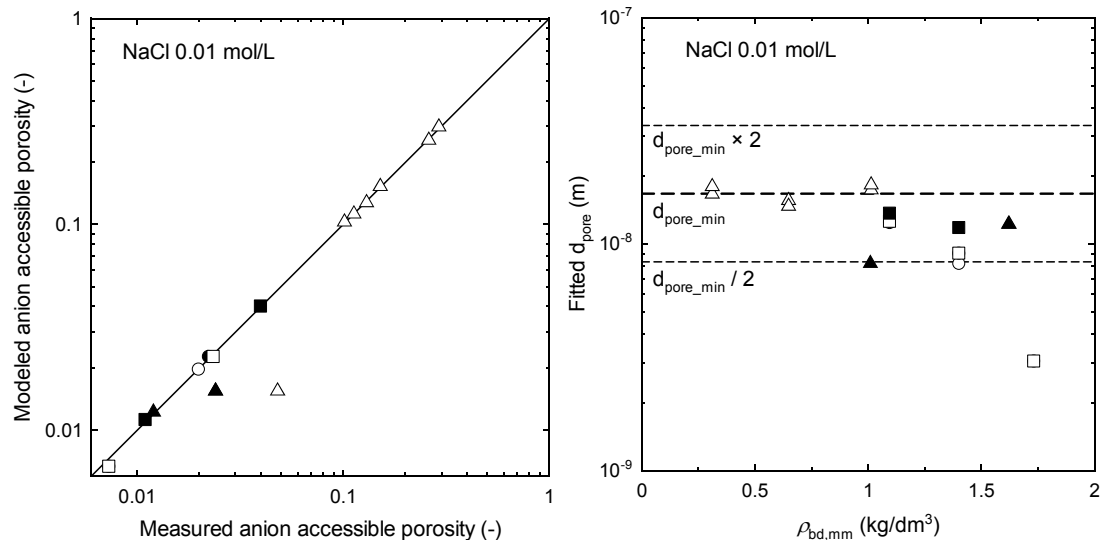


Figure 8. Scheme of montmorillonite microstructure at high density.

1



2



3

4

5 Figure 9. Left: comparison between measured and modelled anion accessible porosity
 6 according to model 4 and a fitted minimum pore size at two ionic strengths. Corresponding
 7 pore sizes are given on the right figures where dash lines are representative of the minimum
 8 pore size value used in Figure 6 (5.5 Debye lengths), and two or half this value.

9

10

11